

## A Numerical Study on the Influence of the Upper Body and Neck on Head Kinematics in Tangential Bicycle Helmet Impact

Florian Feist, Corina Klug

**Abstract** The CEN/TC158/WG11 is developing a new helmet test that takes into account tangential loading. In order to derive a realistic injury risk induced by tangential loading, realistic boundary conditions are essential. However, the influence of the upper body and neck on rotational loading remains unclear.

The aim of this study is to analyse the effect of the upper body and neck in tangential head impact using three state-of-the-art human body models (GHBM, THUMS, CHARM), covering three anthropometric sizes (10-year-old, 5<sup>th</sup> and 50<sup>th</sup> percentile) and two postures (standing, crouching).

A thoroughly validated bicycle helmet model was fitted to the human body models (HBMs). The HBMs were propelled at 6.5 m/s against a flat horizontal anvil. The influence of upper body posture, upper body's compliance and body size was analysed. Simulations were comprehensively evaluated taking into account multiple head injury criteria, contact forces and energy balances.

The data suggest that the contact forces, deformation energy and rotational peak acceleration in isolated head tests are underestimated, while translational accelerations are overestimated. Head velocity change and brain injury criteria (BrIC) are consistent, though. Other head injury criteria in equivalent configurations are different in head-only and full-body impacts.

**Keywords** Brain, Finite Element Methode (FEM), Helmet, Testing, Human Body Models (HBM)

### I. INTRODUCTION

This study is a follow-up to the study published by Klug *et al.* at the IRCOBI Conference 2015 [1]. We exposed six helmet models to frontal and lateral oblique impacts inducing rotational loading. Tests were performed at 6.5 m/s. Helmets were tested considering normal and misuse. We employed a Hybrid III headform in testing. Based on a study by Ghajarij *et al.* [2], the HIII head's inertia and mass were increased, such to account for the influence of the upper body and neck. By means of numerical simulation we further investigated the effects of misuse, skin compliance, anvil angle, anvil type, add-on mass, frictional properties, impact velocity and helmet design parameters. We also investigated various approaches to replicate the effect of the human neck and upper body: a HIII neck with free or guided upper body mass was attached to the headform. We showed that contact forces and rotational velocity change are underestimated and that translational loading is overestimated in head-only testing in comparison to H III head+ HIII neck+ rigid upper body mass. However, the HIII neck is neither designed nor validated for this loadcase.

In the present study we fit the helmet model that was already employed in the previous study to different HBMs. Just like the HIII, HBMs were not originally designed for this loadcase. The premise of the study is to identify trends by applying multiple HBMs, such to derive more sound conclusions and to minimise the risk for drawing wrong conclusions on the effect of the neck and upper body.

#### **Research questions**

- How far apart are results between numerical HBM in tangential head impact?
- What is the influence of the upper body's compliance, i.e. the torso and everything below C7? Can the upper body be simply replaced by a rigid body? Is an accurate neck model attached to a rigid body sufficient to replicate full-body behaviour upon head impact?
- What is the influence of the body size on head loading?
- What is the influence of upper body and neck on head loading? Is the neck and upper body negligible? If so,

Dr. F. Feist (email: florian.feist@tugraz.at; tel: +43 316 873 30312) is Senior Scientist and C. Klug is a PhD student at the Vehicle Safety Institute at Graz University of Technology, Austria.

can we expect the same safety level of helmets tested in isolated head tests?

## II. METHODS

### Numerical Model

The following state-of-the-art HBMs were applied in this study: the Global Human Body Models Consortium (GHBMC) 50th simplified pedestrian, version 1.3; the GHBMC 50th occupant, version 4.3; the Total Human Model for Safety (THUMS) 50th pedestrian and occupant, version 4.02; the THUMS 5th pedestrian, version 4.0; and the Collaborative Human Advanced Research Model – 10 Years old (CHARM 10YO), version 1.0. These models cover three anthropometric sizes (10YO, 5th and 50th) and two shapes (occupant, pedestrian) – see Fig. 1.

Using CHARM, THUMS 50th and 5th isolated head impact tests were performed. The entire body below and including C1 was simply removed. Using THUMS 50th, simulations with a rigidified upper body were performed. The entire body below C7 was turned rigid, not including the torso skin and the muscles (see Fig. 1, right).

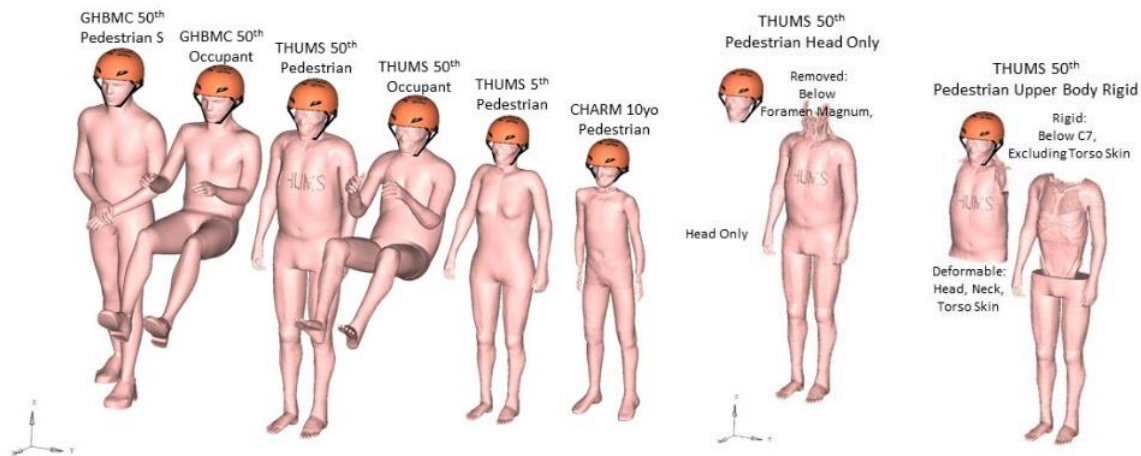


Fig. 1. Human Body Models used in this study.

Two coordinate systems were introduced. First, a helmet coordinate system with an x-y-plane, which is coplanar to the A-A' plane (blue coordinate system in Fig. 2). The coordinate z passes through the point with the largest depth (distance A-A' plane to inner foam liner). Secondly, a HBM coordinate system (red coordinate system in Fig. 2) with an x-y-plane parallel to the Frankfort plane was introduced. The centre of the coordinate system coincides with the head's centre of gravity (CG). The angle enclosed between the two coordinate systems is  $\gamma$  (see Fig. 2 (left), and Table II). The HBM was then oriented relative to the helmet coordinate system such that  $b$ , the eyebrow-to-helmet leading edge distance (see Fig. 2), was 30 mm in adults and 20mm in the pre-adolescent ('two finger rule'). Two helmet sizes were used in the study, size L and size S. The small helmet was simply scaled, applying the headform scaling factors applied in EN 960 (factors used: 1.141, 1.177 and 1.133 in helmet x-, y-, and z-axis). Please refer to Table II in the Appendix for a summary on the fitting parameters for each HBM. Remark on the Frankfort plane: the inferior margin of the orbit was clearly identifiable in all HBMs. The upper margin of the ear canal was not. The upper margin of the mandibular joint head was used instead to establish the Frankfort plane. In CHARM the plane was oriented parallel to the zygomatic process.

In each HBM, consistent accelerometers were introduced: a so-called 'seatbelt accelerometer' is connected to neurocranium through an interpolation constraint. This constraint does not rigidify the cranium. With the interpolation constrained, the motion of a master node (accelerometer) is the averaged motion of all slave nodes (neurocranium). Due to averaging, the signals do not require filtering during post-processing. In the simplified GHBMC pedestrian model, the neurocranium is rigid. Hence, the interpolation constraint was replaced by a rigid body constraint.

All simulations were performed using LS-Dyna MPP R7.1.1 single-precision (except CHARM: double-precision), using eight CPU cores. Control cards were used as supplied with the HBM.

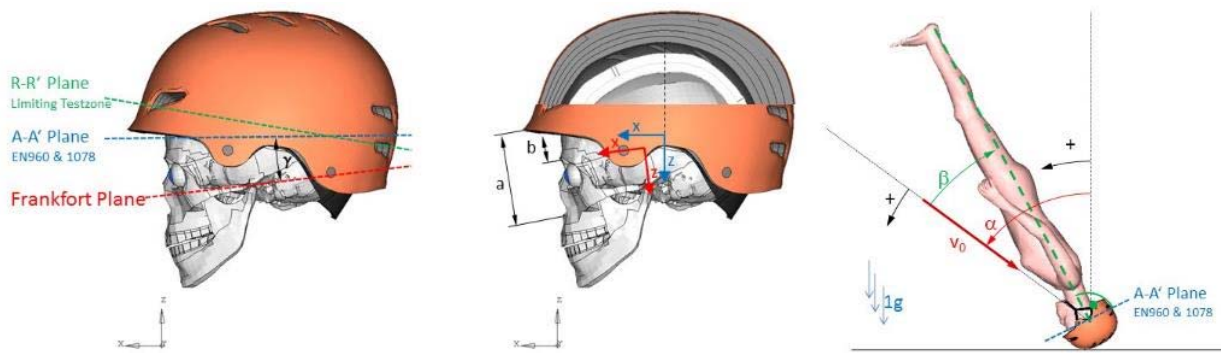


Fig. 2. Impact Orientation (left) and Fitting of Helmet (right).

Once the head was fitted to the helmet, the helmet was oriented relative to the global system (see Fig. 2 (right)). The angle  $\alpha$  is enclosed between the velocity vector and the global vertical axis. The angle  $\beta$  is enclosed between helmet's z-axis and the velocity vector.

In the numerical model a coefficient of friction between helmet and anvil of 0.5 and between helmet and head of 0.35 was chosen, consistent with the validation experiments in the previous study [1].

For a summary on the validation experiments used in the development of the HBM and the helmet model, please refer to the Appendix – sub-chapter ‘Validation of Human Body Models’ and ‘Validation of the Helmet Model’.

**Simulation Matrix**

Using these two orientation parameters, i.e.  $\alpha$  and  $\beta$ , a simulation matrix was established (see Fig. 3). The green and blue digits form the Run-ID. The first two digits (green numbers) are referring to the impact constellation, while the last two digits refer to the HBM used.

An example: Run 1213 is a run with a velocity vector rotated by  $\alpha=30^\circ$ . The helmet (and thus the HBM) is rotated by another  $\beta=15^\circ$  relative to the velocity vector. In Run 1213 a 5th THUMS pedestrian is used.

In the previous study we had shown that an impact angle (or anvil angles) of  $30^\circ$  showed a good trade-off between rotational and translational loading. In CEN/TC158/WG11 an impact angle between  $30^\circ$  and  $60^\circ$  is under discussion [3], with a tendency toward  $45^\circ$  [4],[5]. Here, the simulation matrix covers impact velocity angles between  $30^\circ$  and  $45^\circ$ . Also, the simulation matrix covers pitched impacts, i.e. where the impact point is more to the front, to the side or to the top ( $\beta < > 0$ ).

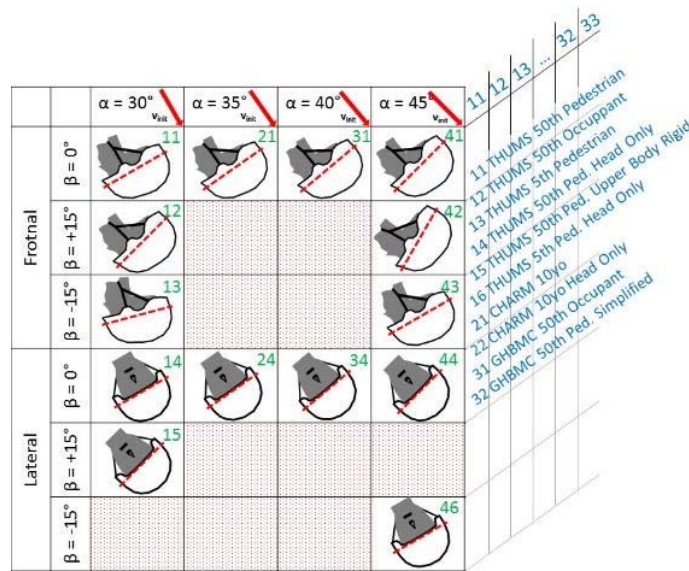


Fig. 3. Simulation Matrix.

Given the large output of the roughly 140 simulations, we did not analyse the vectorial data (time curves) case-by-case, but analysed scalar data (HIC, peak acceleration,...) by means of statistics. The simulations cover a set of

14 impact scenarios, which are considered as relevant in future tangential head impact testing (CEN). We take the assumption that the overall trends indicated by the entire simulation-set are conclusive.

Simulations were evaluated in terms of rotational and translational loading (peak acceleration and velocity), as well as a variety of injury criteria: Head Injury Criterion (HIC), Brain Injury Criterion (BrIC), Power Index (PI) and Kleiven Criterion (KLC, sometimes also referred as Kleiven Linear Combination). The numerical brain model was post-processed by applying the cumulative strain damage measure (CSDM) and maximum principal strain (MPS) to the brain tissue. For a detailed description of the criteria refer to [1].

### III. RESULTS

#### THUMS 50th P and GHBMC 50th PS

The bars in the diagrams show the median value of the 14 impact configurations. The error bars indicate the 5th and 95th percentile values. Units in diagrams, unless denoted differently, are  $\text{rad/s}^2$ ,  $\text{rad/s}$ ,  $g$ ,  $\text{kN}$  and Joule for rotational acceleration, velocity, translational acceleration, force and energy, respectively.

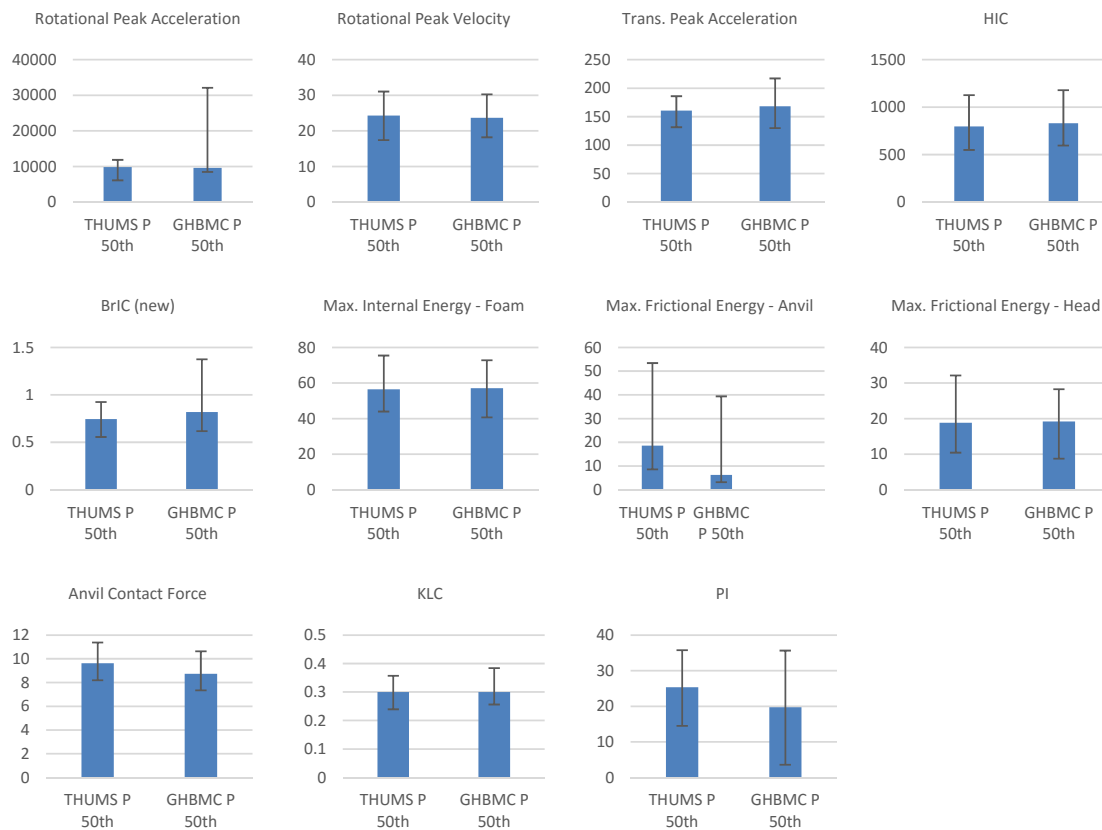


Fig. 4. Comparison Full-Body Impacts with THUMS and GHBMC 50th Pedestrian.

The comparison between THUMS and GHBMC shows that both models respond to the tangential head impact consistently (see Fig. 4). Except for the PI and the friction energy (helmet-anvil), all injury criteria show quite similar values. Differences, e.g. in the frictional energy between helmet and anvil, are likely caused by the different neck postures. Initial distance between chin and sternum is smaller in THUMS (see Fig. 5 at T=0 ms). This leads to an earlier rotational constraint (see Fig. 5, at T=10 ms), eventually leading to higher frictional energies and anvil contact forces. Still, results match fairly well, and overall the behavior of the models is consistent in terms of loading and kinematics (see Appendix).

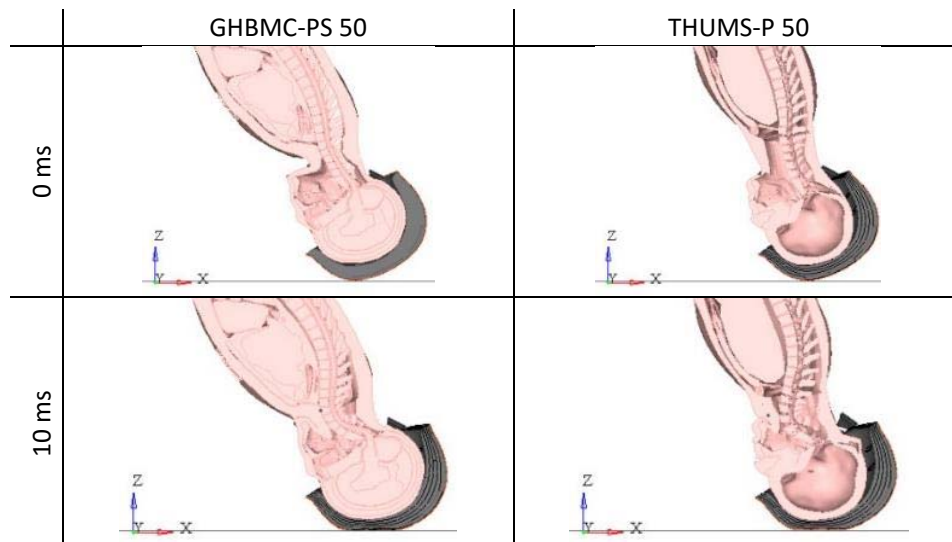


Fig. 5. ‘Short neck’ THUMS versus ‘long neck’ GHBMC – cross-section – Run 1111 versus 1132 t=0 and 10 ms.

**Head-only and Full-Body Simulations for varying anthropometric sizes**

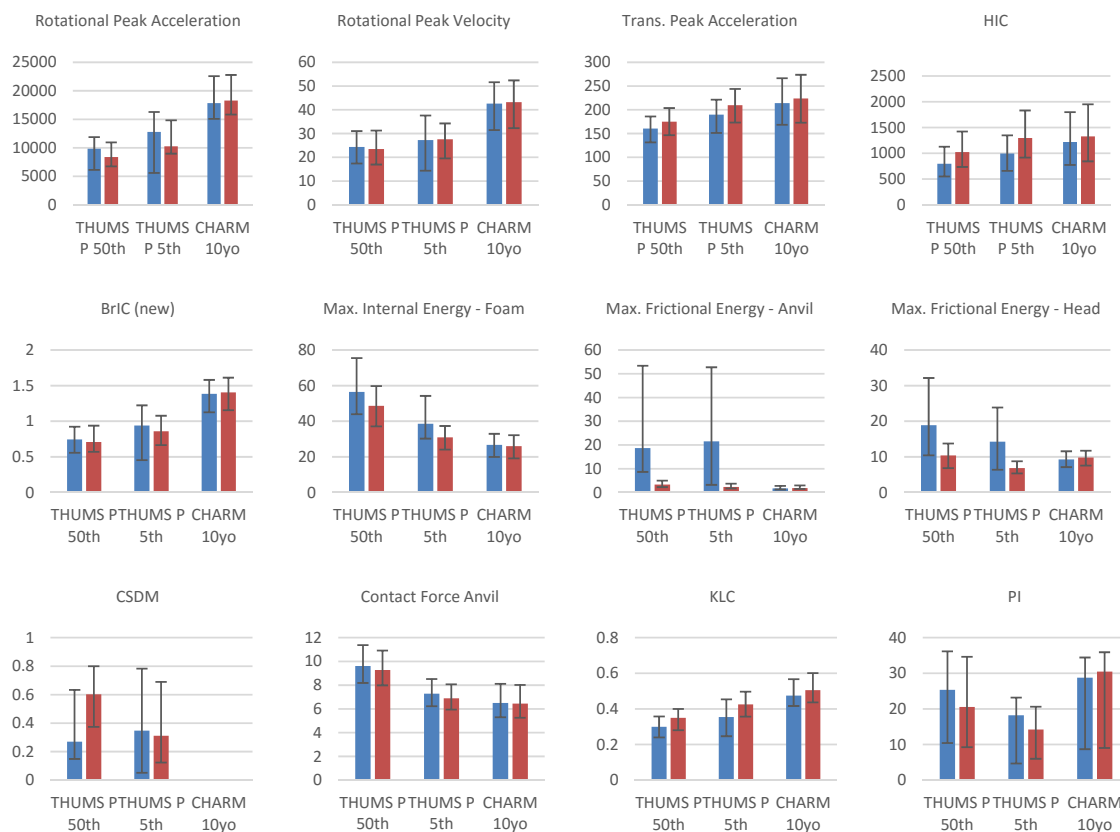


Fig. 6. Comparison Full-Body and Isolated Head Impact Test. ■ Head+Upper Body ■ Head Only

Comparison of rotational velocity change shows that head-only and full-body simulations return similar results (Fig. 6). Consequently, BrIC is fairly similar, too. In terms of translational peak accelerations, though, isolated head tests tend to overestimate. As a result, injury criteria which are entirely or partly based on translational acceleration signals are overestimated in isolated head tests, such as HIC and KLC. In Power Index (PI), the effect of very mildly reduced rotational acceleration seemingly overrules the effect of raising translational acceleration and PI tends to be smaller in isolated helmet tests.

In energy balance we find huge differences in full-body and isolated head tests. Maximal internal energy, i.e. the energy that is ‘stored’ in the foam material, is underestimated with isolated heads. Seemingly, the differences become larger the larger the pedestrian. Same with the dissipative frictional energies. To our understanding, this also means that the frictional properties of the outer shell play an ever larger role in real-world accidents than in lab-environment tested helmets with isolated heads.

Evaluation of the Cumulative Strain Damage Measure (CSDM) showed a huge increase in isolated head tests in THUMS 50th, while in THUMS 5th the CSDM rather decreased. Possible reasons for these opposing trends are summarised in the Discussion, below.

In our previous paper we had artificially increased impactor mass in testing, such to account for the upper body. If that approach holds true, we should find an increased effective mass in full-body simulations. In the bar diagrams, differences seem rather negligible. However, when correlating contact force and acceleration, we find the mass in the linear regression curve (5.4 kg in THUMS 50th and 3.37 kg in THUMS 5th – see Fig. 7, red curves). Indeed, the regression parameter, i.e. the effective mass, of the whole-body simulations are roughly 15% higher (blue curves), suggesting, for example, an effective mass of 6.27 kg for the 50th adult.

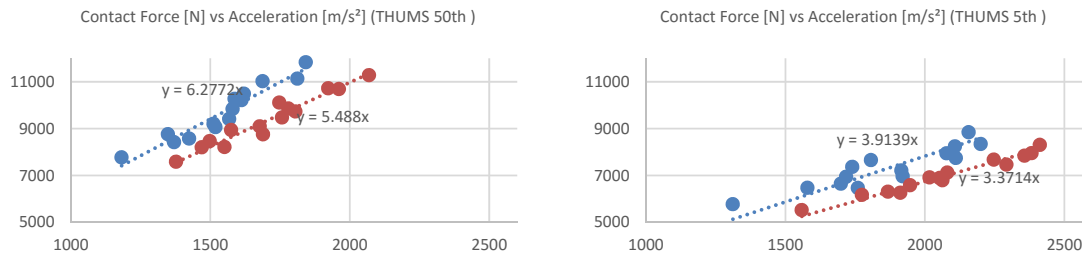


Fig. 7. Contact Force vs Acceleration ( $R^2 > 0.92$ ). ■ Head+Upper Body ■ Head Only

Correlating rotational peak acceleration versus tangential anvil force did return a very low coefficient of determination, R-squared (0.1) – see Fig. 8.

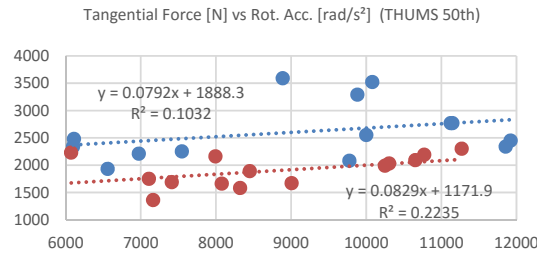


Fig. 8. Tangential Force versus Rotational Acceleration. ■ Head+Upper Body ■ Head Only

We grouped our numerical simulations by impact type (lateral/frontal) and size (50<sup>th</sup> and 5<sup>th</sup>). To obtain a scaling factor for  $I_{xx}$ , and  $I_{yy}$  the ratio of rotational acceleration between full body and head-only simulations was calculated. Fig. 9 shows the average scaling factors for THUMS 50<sup>th</sup> and 5<sup>th</sup>, both, in frontal and lateral impact. Table I summarizes the p-values when comparing the groups ‘full-body’ with ‘head-only’. The low p-values suggest that the difference between both groups in terms of rotational peak acceleration are statistically significant (Table I, 1<sup>st</sup> row). The analysis suggests a scaling factor of 1.2 in frontal impact ( $I_{yy}$ ) for both, THUMS 50<sup>th</sup> and 5<sup>th</sup>. In lateral impact ( $I_{xx}$ ) scaling factors amount for 0.9 in THUMS 50<sup>th</sup> and 0.6 in THUMS 5<sup>th</sup>. Generally, the ratios for single component acceleration (x-,y- acceleration, blue bars) and resultant acceleration (red bars) were found to be fairly similar.

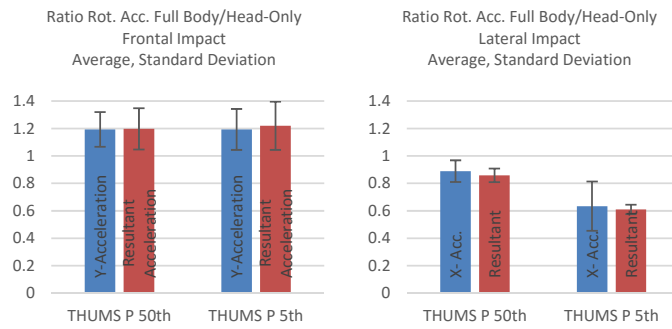


Fig. 9. Ratio between Full-Body and Head-Only Simulation in terms of Rotational Acceleration in Frontal and Lateral Impact

In terms of rotational velocity (Table I, 2<sup>nd</sup> row), p-values of a paired two tailed Student’s t-test were very high, suggesting that the difference between the groups (‘full body’ and ‘head only’) are not statistically significant.

TABLE I

	p-values of paired two-tailed Student t-test when comparing group ‘full-body’ with group ‘head-only’							
	Frontal Impact				Lateral Impact			
	THUMS 50th		THUMS 5th		THUMS 50th		THUMS 5th	
	Y	Resultant	Y	Resultant	X	Resultant	X	Resultant
Rotational Acceleration	0.000	0.002	0.006	0.007	0.016	0.001	0.013	0.000
Rotational Velocity	0.846	0.232	0.007	0.051	0.296	0.859	0.244	0.104

**Crouching and Standing Posture**

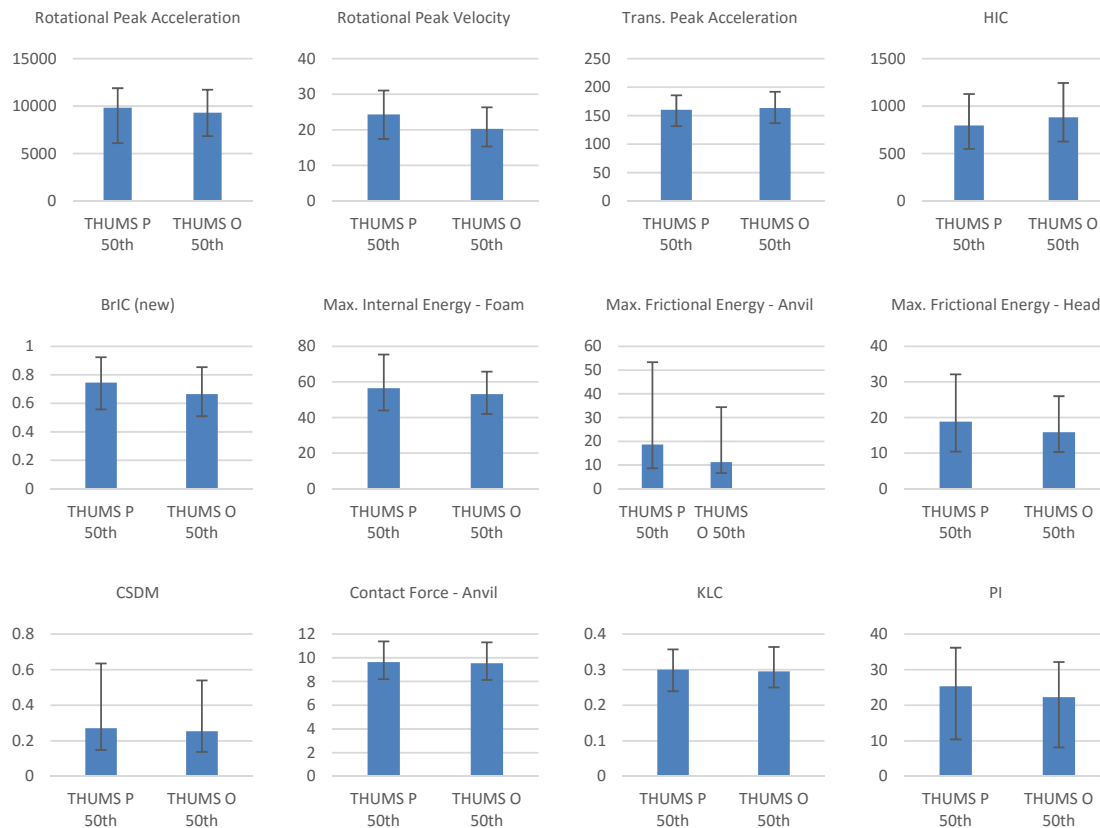


Fig. 10. Comparison of Standing and Crouching.

The crouching of the pedestrian seems to reduce effective mass slightly. As a result, translational acceleration and HIC are slightly higher and contact force is slightly smaller. In the bar diagrams this is hardly perceivable. It becomes more obvious when correlating contact force and translational peak acceleration. In

crouched position the effective mass is approx. 10% higher than in head alone simulations, and 5% smaller than in standing position.

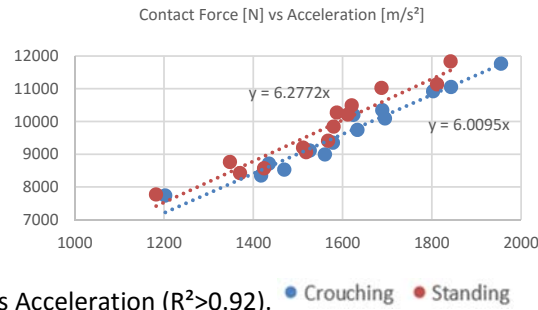


Fig. 11. Contact Force versus Acceleration ( $R^2 > 0.92$ ). ● Crouching ● Standing

Consistently in the observations with the isolated head, the HIC was larger, and the BRIC, PI, Frictional Energies and Internal Energies were smaller in the crouched position.

The error bars, which are indicating the spread of the data, are larger in the pedestrian. This means that in standing position the loads are more sensitive to the impact configuration.

**Rigidified upper body**

Simulations with a rigidified upper body resulted in a complete change in model response. Rotational and translational accelerations, as well as rotational peak velocity, were extremely increased. Fig. 12 shows a comparison of deformable and rigid upper body for four selected runs (frontal impact: 11, 41, lateral impact: 14, 44).

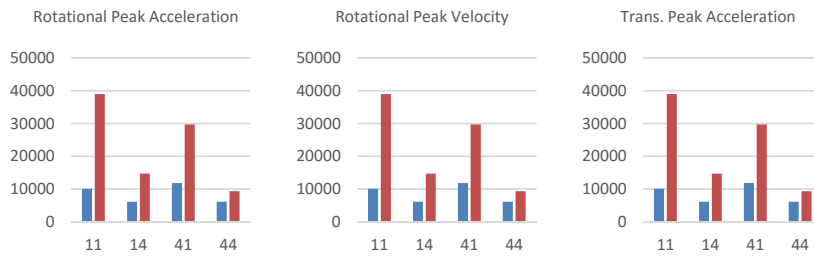


Fig. 12. Deformable versus Rigid Upper Body (below C7) for selected runs. ■ Deformable UB ■ Rigid UB

Fig. 13 shows the effect of thoracic and lumbar spine on overall response in a selected impact configuration. Thoracic and lumbar spine show significant bending in the non-rigidified HBM.

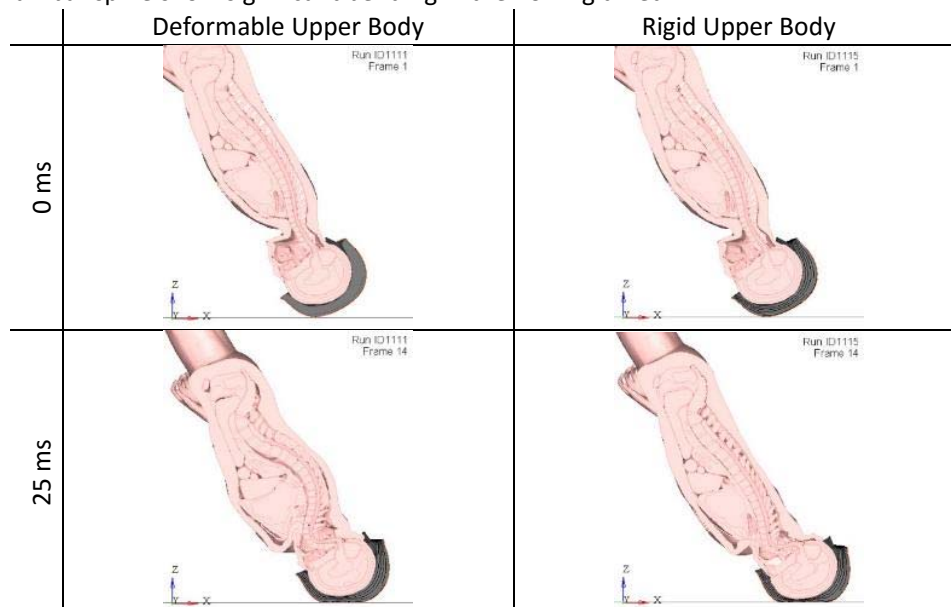


Fig. 13. Deformable versus Rigid Upper Body (below C7) – cross-section – t=0 and 25 ms.

### Kinematics in Full-Body Simulations

Impact configuration 11 (compare simulation matrix in Fig. 3) was selected for a visual comparison and analysis of kinematics. For a full side-to-side visual comparison, refer to the Appendix (see Fig. 19 through Fig. 22; Remark: CHARM 10YO simulations are not shown up to 25 ms, as starting with 10 ms unrealistic penetrations occur).

At 6 ms, first extension in the cervical spine can be seen (see Fig. 14(A)). At 8–9 ms, C1 contacts the occiput and its rotation is arrested (see Fig. 14 (B)). First flexion of the thoracic spine can be seen. At 10ms, the chin starts to contact the chest (in the ‘short’ necked THUMS) or the throat (in the ‘long’ necked GHMBC). In CHARM 10YO we find penetrations between mandibular and the spine (see Fig. 14 (C)). At 20ms, the mandibular is pushed behind the sternum in THUMS 50<sup>th</sup> and 5<sup>th</sup> (see Fig. 14 (D)). Please refer to Fig. 23 through Fig. 26 in the Appendix for full-body kinematics in all 14 impact scenarios.

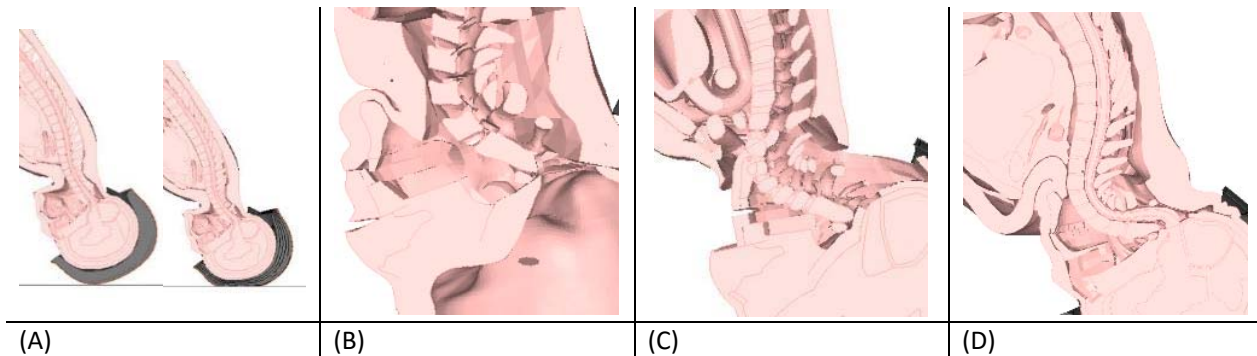


Fig. 14. Selected simulation frames.

## IV. DISCUSSION

### Strains in Brain Matter

The CSDM values in the detailed 50<sup>th</sup> THUMS were remarkably higher in head-only simulations. This was not the case in THUMS 5<sup>th</sup> (Fig. 6). The diverging trends are likely caused by the different brain models. The newer THUMS 50<sup>th</sup> v 4.02 is using a supposedly advanced brain model, with a much finer discretisation: element size was reduced to as little as 1.2mm [6] and number of elements was octuplicated. The biofidelity in terms of displacement of the advanced brain model is said to be reasonable in the centre, but poor at the “outer side of the brain” [7],[8]. The interface between brain and CSF is realised through shared nodes, while this is not the case for the falx. This may result in stress and strain hotspots near the brain’s outer surface. Indeed, the maximum principal strains in THUMS 50<sup>th</sup> are rather located near the brain surface, while located near the brain centre (pons, ventricles) in THUMS 5<sup>th</sup>.

In THUMS 50<sup>th</sup> v4.02 the brainstem continues with the spinal cord, which is not modelled in THUMS 5<sup>th</sup> v4.0. Removing the spinal cord in the head-only simulations in THUMS 50<sup>th</sup> might change the boundary conditions near the foramen magnum. A visual side-by-side comparison of the maximum principal strain does not show significant strains in the brainstem nor major differences in strain-level with and without upperbody (Fig. 15). We therefore assume that removing the upper body did not affect the boundary conditions at the foramen magnum in THUMS 50<sup>th</sup> v4.02.

Comparison between THUMS 50<sup>th</sup>, THUMS 5<sup>th</sup> and GHMC-O 50<sup>th</sup> shows substantial differences in strain level and even more strain location (Fig. 15 through Fig. 16, and Fig. 27 through Fig. 30 in the Appendix) in frontal impact. In THUMS 5<sup>th</sup> the Maximum Principal Strain (MPS) is located in the brain stem, which seems to move freely and unconstrained at the foramen magnum. Given the small relative volume of the brainstem, though, the effect on CSDM evaluation is limited. When disregarding the brain stem in THUMS 5<sup>th</sup> (with MPS exceeding 100%), the strain levels are smaller compared to the other HBMs (therefore CSDM 20% was based on 10% strain in Fig. 6 for THUMS 5<sup>th</sup>). Aside the MPS hotspots in the brainstem, MPS is rather located near the pons. In THUMS 50<sup>th</sup> and GHMBC 50<sup>th</sup> the brainstem shows rather small strain levels. In THUMS 50<sup>th</sup> MPS is rather located near the brain surface, in GHMBC 50<sup>th</sup> near to the coup. The same observations can be made in other impact scenarios too (see Appendix, Fig. 27). In lateral impacts (see Appendix, Fig. 29 and Fig. 30) strain pattern/distribution is more

consistent between models (when comparing GHBM and THUMS v4.02). Remarkable is the much more pronounced (and visible) deformation along the falx cerebri in THUMS v4.02.

The morphological difference between the brain in THUMS and GHBM are quite large, in particular in the region of the temporal lobe (Fig. 15) and in the cerebellum (Fig. 29 in the Appendix).

A short remark on Fig. 15: Critical values for MPS published in literature are covering a large range: For THUMS Kitagawa et al. [9] suggests 20% for diffuse axonal injury. Watanabe et al. suggests 30% for "brain tissue damage and cerebral contusion" [10]. For GHBM Takhounts et al. [11] provided risk curves, with a MPS of 50% roughly equalling a 50% risk for AIS2. For Fig. 15 an intermediate value (35%) was deliberately selected to allow for a side-to-side comparison of all models.

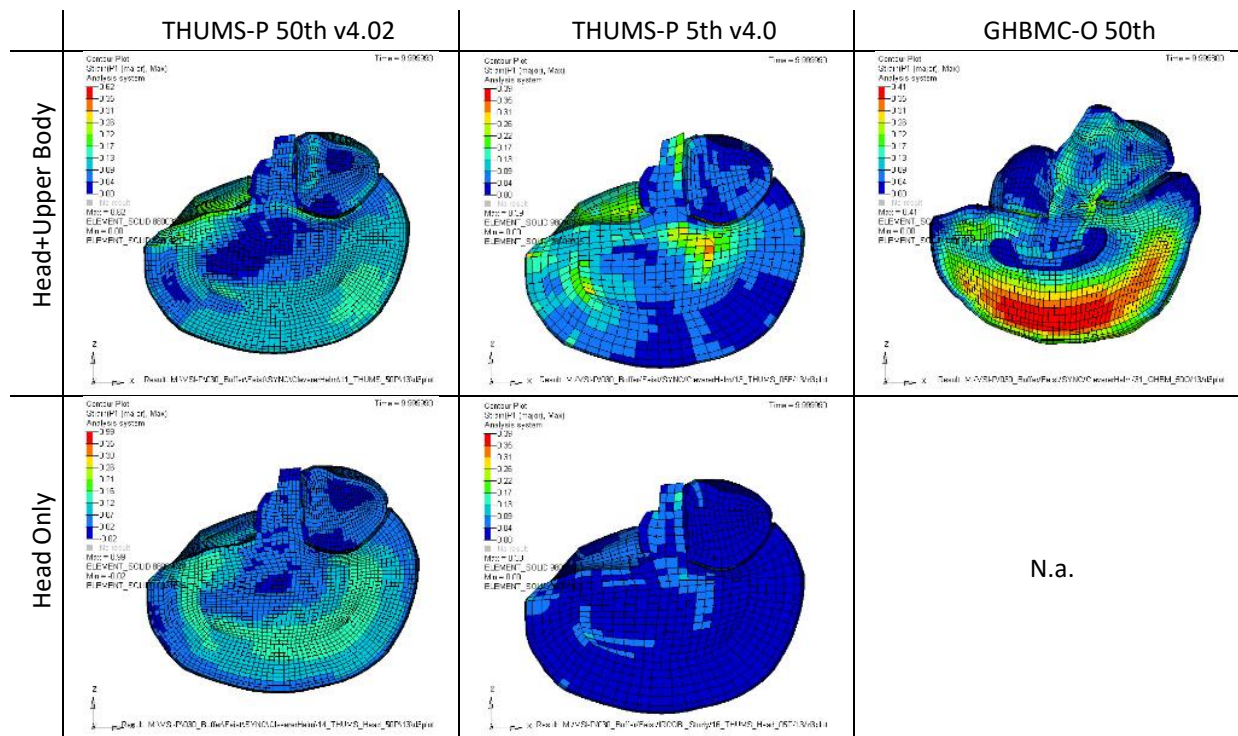


Fig. 15. Maximum Principal Strain in three different HBMs at 10 ms (Run 13)

Fig. 16 shows the MPS at a later stage of the impact (25 ms). In THUMS 50<sup>th</sup>, the strain level, and localization of strain is quite consistent in the first 10-15 ms (in full body and head-only simulations) – see Fig. 15. Then the strains are increasing in the head-only simulations.

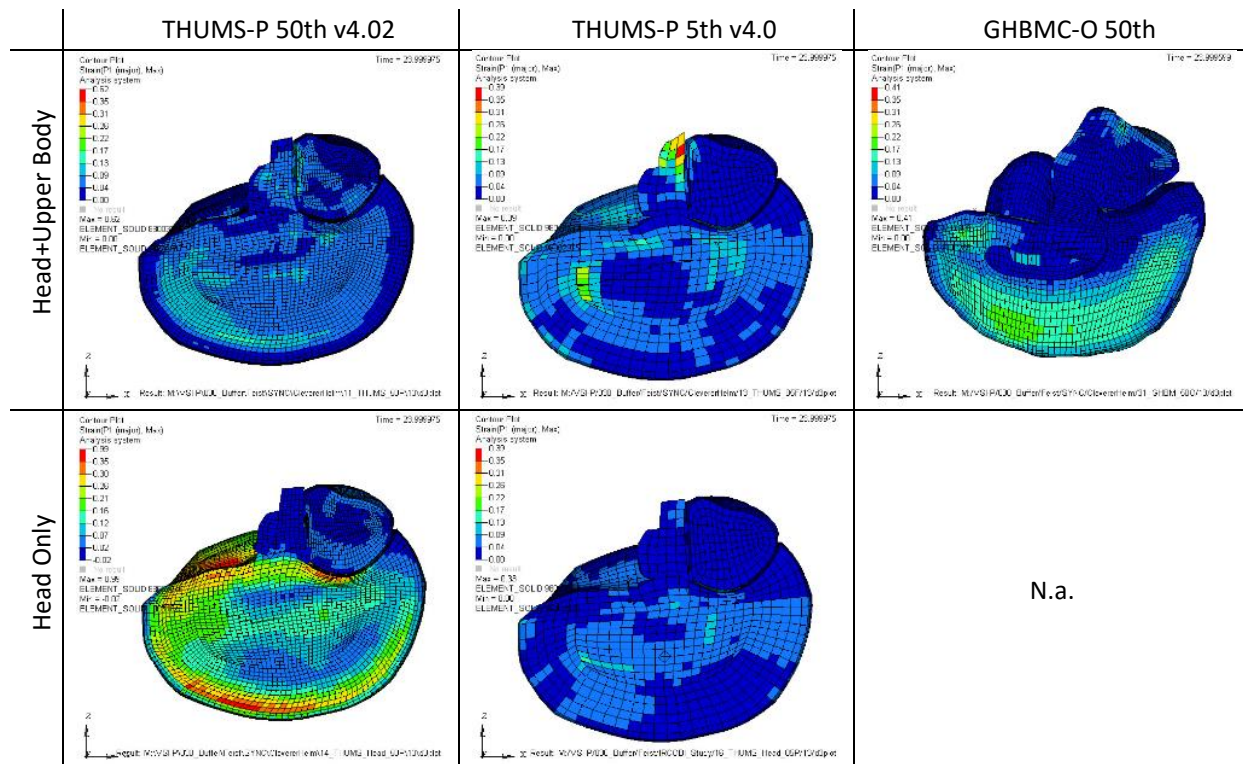


Fig. 16. Maximum Principal Strain in three different HBMs at 24 ms (Run 13)

The THUMS v4.02 brain consists of 200,000 elements. Element-Output files for CSDM evaluation quickly become cumbersome and time-consuming to analyse: at a frequency of 10kHz, the file size gains 10 GB for 25 ms simulation time. With v4.02 we had to cut analysis frequency to 1 kHz for the ease of post-processing.

**Effect of Upper Body**

Morphological differences in THUMS and GHBMC are not limited to the brain and result in different chin-to-chest interaction. THUMS has a rather short neck, which means, that head rotation is suspended earlier and that more impact energy is converted to frictional energy. Generally, the models show rather little anatomical detail in the anterior neck region (missing thyroid gland, trachea, oesophagus). We cannot estimate whether these simplifications are detrimental to the models’ fidelity in tangential head impact.

The presence of an upper body had huge effects on the maximal frictional energy between helmet and anvil. Helmet innovations that try to enhance protection through low-friction covers (e.g. Lazer Superskin) should be evaluated considering the upper body in any case, e.g. in a separate abrasion test.

The maximal deformation energy was higher in fully body simulations. The helmet deforms more, which causes lower HIC and lower peak translational acceleration (as long as the foam does not bottom out).

Generally, spread of results in full-body simulation was larger than in isolated head tests.

A correlation of impact force and acceleration showed that the effective impact mass is 15–20% higher in full-body impacts. The amount of increase in effective mass depends on the posture of the cyclist: crouching (15%) or standing (20%). The robustness of this finding was shown by applying multiple HBMs. The study supports findings from Ghajari *et al.* [2], who proposed a mass scaling between 15% and 19% depending on the tangential velocity for impacts with a normal velocity of 7.5 m/s for 60° impacts.

In terms of inertia properties, Ghajari *et al.* [2] concluded that the three diagonal components of the inertia tensor need to be scaled independently and that the scaling factors are time variant. Eventually, they proposed to scale  $I_{xx}$  and  $I_{yy}$  by the time peak, i.e. by 0.69 and 1.4, respectively. We found similar values, suggesting a scaling factor of 0.6 to 0.8 for  $I_{xx}$  and 1.2 for  $I_{yy}$ . For  $I_{yy}$  the scaling factor was independent of HBM size, while for  $I_{xx}$ , a smaller scaling factor was found for the smaller THUMS 5<sup>th</sup>.

In terms of maximum rotational velocity, there were marginal differences observed between head-only and full-body simulations (Table I). Now, to compensate for the missing upper body, the inertia must be adjusted in head-only tests to gain an identical rotational acceleration. But, this would change the rotational peak velocity

(increased velocity about x-axis, decreased about y-axis). We therefore hypothesize that a simple head-only test can only simulate the full-body impact in terms of rotational peak velocity or rotational peak acceleration, unless the centre of gravity is tweaked (e.g. different headforms for frontal and lateral impact).

This means, that prior to the definition of the headform specifications (mass, inertia, location of CoG) or even the general test setup, the injury risk assessment method has to be selected: If head injury is assessed by means of rotational peak acceleration, the inertias need to be adjusted. If head injury is assessed by means of rotational velocity change (e.g. BRIC), the inertia must not be changed. If head injury is assessed by means of translational acceleration (e.g. HIC), the mass needs to be increased, which will affect inertia too (parallel axis theorem). This means, that with a head-only test it has to be decided which is the most relevant (injury producing) load measure.

Kleiven [12] reported that HIC can predict the strain level in the brain of a finite element (FE) model for purely translational impulses of short duration, while the peak in angular velocity showed better correlation with the strain levels in an FE head model for purely rotational impulses than angular accelerations or HIP. Moreover, Mordaka, Kleiven et al. [13] evaluated the relationship between head kinematics and injury, suggesting that angular velocity components better correlated to mTBI than angular acceleration. The importance of rotational velocity for producing strains in the brain is further underlined by the development history of BRIC [14], which originally contained a term including the rotational acceleration, but which now is simply based on rotational peak velocity [11]. We therefore conclude, that the maximum rotational velocity is more relevant for brain injury prediction.

An isolated head helmet-test is simple, robust and economically reasonable. So there are many aspects speaking for a head-only test. If the test fails in replicating a full-body test, we propose to scale the measurements ex-post, i.e. rotational peak acceleration and translational peak acceleration are scaled based on numerical simulations using HBMs. Given the limitations of a simple head-only test, the application of sophisticated finite-element based injury risk assessment tools seem well-intentioned, but questionable.

We had expected that the upper body adds comparatively little to the overall body compliance in comparison to the neck. Simulations with the rigid upper body showed clearly the dissipative effects of the thoracic and even lumbar spine. This means that a very accurate model of the cervical spine is not sufficient for accurate oblique head impact simulations, since the entire spine is of importance for the model's response.

To summarise, the study clearly shows the importance of considering the upper body and neck for helmet tests, which is consistent with findings in previous studies [2],[15].

### ***Effect of Size***

Higher values for all kinematic injury criteria were observed for simulations with the lighter and smaller HBMs, i.e. THUMS 5th and CHARM. This effect was observed for both translational and rotational loads, in simulations with head-only and full-body. Foam density remained unchanged in these simulations, i.e. the same foam was used in small and large helmet.

Results obtained with CHARM 10YO were included in the diagrams but not further discussed in the result section. In CHARM 10YO v1.0, the neck appears incomplete. The neck currently consists of 1D element muscles and the spine. Neck soft tissue is missing. Also, the model shows penetration of head and neck. We were only able to run CHARM 10YO with the double precision solver. Still, CHARM 10YO is a valuable contribution of Wayne State University for expanding our knowledge in injury in pre-adolescents and we are looking forward to using updated versions.

### ***Effect of Impact Configuration***

The simulation matrix contained a set of tangential head impact configurations. Considering all the data in this study, it is surprising that head loads and associated injury criteria cover such wide ranges. Considering the isolated head impact tests to just one single point on the helmet, i.e. Run IDs 1114, 1116, 1122, 4314, 4316, 4322, we obtain, for example, a HIC range of 806–1764 and a BRIC range of 0.65–1.67.

The spread of the data, are larger in the pedestrian. This means that in standing position the loads are more sensitive to the impact configuration.

### ***Limitations***

- Simulations were performed up to 25 ms after impact. All evaluation is limited to that time span.
- THUMS v4 was developed in LS-Dyna R3 [6], GHBM was developed in LS-Dyna R6.1 [16]. We conducted

simulations in a different environment and were using a different LS-Dyna release, namely R7.1.1. Environment and release can have an influence on the model's behaviour.

- We put efforts in consistent fitting of helmets to the different HBM (see Fig. 2), orienting the helmet relative to Head COG and Frankfort plane (compare Table II). We used the models as supplied and did not reposition or remesh the models. As a consequence postures of models may be not entirely consistent (initial neck flexion, position of limbs,...).

## V. CONCLUSIONS

- Simulations show that head loading not only depends on neck kinematics but also to a good extent on thoracic and even lumbar spine impact responses. This means that an accurate neck model is not enough for accurate head impact simulations.
- Simulation with THUMS and GHBM of the same anthropometric size showed consistent results in terms of kinematics. Only minor differences of the evaluated kinematic injury criteria were observed. Such differences were mainly caused by morphological differences in THUMS and GHBM (e.g. chin-chest interaction).
- Strains in brain matter of THUMS 50<sup>th</sup>, 5<sup>th</sup> and GHBM 50<sup>th</sup> were quite different in terms of level, localization and transient behaviour. Sound conclusions on the effect on brain strains when neglecting the upper body in helmet tests can not be drawn, since results were contradicting.
- Anthropometric size clearly influences the results for simulations with and without upper body. Head mass and head inertia have a considerable effect on rotational and translational head loading (under the assumption that the density of the energy-absorbing foam remains unchanged).
- In full-body impacts the helmet's foam has to absorb 15–20% more energy.
- In full-body impacts the friction energy is way larger. The shell has to handle larger frictional energies.
- In full-body impacts the translational peak accelerations are smaller and rotational peak accelerations are higher. However, rotational peak velocity is consistent in full-body and head-only impacts.
- Numerical simulations with a variety of HBMs show that the effective impact mass is 10–15% higher in full-body simulations in comparison to head-only simulations.
- To replicate rotational peak velocity the inertia must not be changed. To replicate rotational peak acceleration, though, the inertia needs to be increased by 20% about y-axis, and decreased by 20-40% about x-axis (depending on size of the HBM).

## VI. ACKNOWLEDGEMENTS

The authors would like to acknowledge the use of HPC resources provided by the ZID at Graz University of Technology, Austria. The authors thank Wayne State University for providing the CHARM-10 models free of charge. The authors acknowledge that Elemance LLC is the exclusive distributor of the Global Human Body Model Consortium-owned GHBM-Model. The authors acknowledge that Toyota Motor Corporation and Toyota Central R&D labs, Inc., are the owners of the licensed Total Human Body Model for Safety.

## VII. REFERENCES

- [1] Klug, C., F. Feist, and E. Tomasch. (2015) Testing of bicycle helmets for preadolescents. *IRCOBI Conference Proceedings*, pp. 136–155
- [2] Ghajari, M., S. Peldschus, U. Galvanetto, and L. Iannucci. (2013) Effects of the presence of the body in helmet oblique impacts. *Accident; analysis and prevention* 50:263–271
- [3] Halldin, P. CEN/TC 158 - WG11 Rotational test methods. New Orleans, USA, 2014. [http://www.sis.se/PageFiles/2528/WG11\\_Status\\_report\\_141105.pdf](http://www.sis.se/PageFiles/2528/WG11_Status_report_141105.pdf). Accessed 1 June 2016
- [4] Willinger, R., C. Deck, P. Halldin, and D. Otte Towards advanced bicycle helmet test methods. *International Cycling Safety Conference 2014*,
- [5] Stigson, H., and A. Kullgren Folksam's Bicycle Helmet Test 2015 Helena Stigson. (2015)
- [6] Toyota Motor Corporation Documentation Total Human Model for Safety (THUMS): AM50 Pedestrian/Occupant Model Academic Version 4.02\_20150527. (2015)

- [7] Iwamoto, M., Y. Nakahira, and H. Kimpara. (2015) Development and Validation of the Total Human Model for Safety (THUMS) Toward Further Understanding of Occupant Injury Mechanisms in Precrash and During Crash. *Traffic injury prevention* 16 Suppl 1:S36-48
- [8] Iwamoto, M., and Y. Nakahira. (2015) Development and Validation of the Total Human Model for Safety (THUMS) Version 5 Containing Multiple 1D Muscles for Estimating Occupant Motions with Muscle Activation During Side Impacts. *Stapp car crash journal* 59:53–90
- [9] Kitagawa, Y., and T. Yasuki (2014) Development and Application of THUMS Version 4. *5th International Symposium: Human Modeling and Simulation in Automotive Engineering*, 2014, Munich, Germany.
- [10] Watanabe, Y., H. Ichikawa, O. Kayama, K. Ono, K. Kaneoka, and S. Inami Relationships Between Occupant Motion and Seat Characteristics in Low-Speed Rear Impacts, 1999-01-0635. SAE International. Warrendale, PA. <http://papers.sae.org/1999-01-0635/>. (1999. Accessed 30 July 2015
- [11] Takhounts, E.G., M.J. Craig, K. Moorhouse, J. McFadden, and V. Hasija. (2013) Development of brain injury criteria (BrIC). *Stapp car crash journal* 57:243–266
- [12] Kleiven, S. (2005) Influence of Direction and Duration of Impacts to the Human Head Evaluated Using the Finite Element Method. *2005 IRCOBI Conference Proceedings*, 2005, Prague, Czech Republic.
- [13] Mordaka, J., S. Kleiven, van de Schijndel-de Nooij, Margriet, R. de Lange, L.J.G. Casanova, E. Carter, and H. von Holst The Importance of Rotational Kinematics in Pedestrian Head to Windshield Impacts. *International Research Council on the Biomechanics of Injury (Hg.) 2007 – 2007 IRCOBI Conference Proceedings*, pp. 83–94
- [14] Takhounts, E.G., V. Hasija, S.A. Ridella, S. Rowson, and S.M. Duma Kinematic rotational brain injury criterion (BRIC). *Proceedings of the 22nd International Technical Conference on the Enhanced Safety of Vehicles (ESV)*,
- [15] Walsh, E.S., M. Kendall, B.T. Hoshizaki, and M.D. Gilchrist (2014) Dynamic Impact Response and Predicted Brain Tissue Deformation Comparisons for an Impacted Hybrid III Headform With and Without a Neckform and Torso Masses. *2014 IRCOBI Conference Proceedings*, 2014, Berlin, Germany.
- [16] Gayzik, S. User Manual: M50 Occupant Version 4.3 for LS-DYNA. Global Human Body Models Consortium, LLC. (2014. Accessed 3 June 2016
- [17] Mao, H., L. Zhang, B. Jiang, V.V. Genthikatti, X. Jin, F. Zhu, R. Makwana, A. Gill, G. Jandir, A. Singh, and K.H. Yang. (2013) Development of a finite element human head model partially validated with thirty five experimental cases. *Journal of biomechanical engineering* 135(11):111002-1-15
- [18] Trosseille, X., C. Tarrière, F. Lavaste, F. Guillon, and A. Domont (1992) Development of a F.E.M. of the Human Head According to a Specific Test Protocol. *36th Stapp Car Crash Conference Proceedings*, 1992, Seattle, Washington, USA.
- [19] Nahum, A.M., R. Smith, and C.C. Ward (1977) Intracranial Pressure Dynamics During Head Impact. *21st Stapp Car Crash Conference Proceedings*, 1977, New Orleans, LA.
- [20] Hardy, W.N., M.J. Mason, C.D. Foster, C.S. Shah, J.M. Kopacz, K.H. Yang, A.I. King, J. Bishop, M. Bey, W. Anderst, and S. Tashman. (2007) A Study of the Response of the Human Cadaver Head to Impact. *Stapp car crash journal* 51:17–80
- [21] Hardy, W.N., C.D. Foster, M.J. Mason, K.H. Yang, A.I. King, and S. Tashman. (2001) Investigation of Head Injury Mechanisms Using Neutral Density Technology and High-Speed Biplanar X-ray. *Stapp car crash journal* 45:337–368
- [22] Hodgson, V.R., J. Brinn, L.M. Thomas, and S.W. Greenberg (1970) Fracture Behavior of the Skull Frontal Bone Against Cylindrical Surfaces. *14th Stapp Car Crash Conference Proceedings*, 1970
- [23] Yoganandan, N., F.A. Pintar, A. Sances, JR, P.R. Walsh, C.L. Ewing, D.J. Thomas, and R.G. Snyder. (1995) Biomechanics of skull fracture. *Journal of neurotrauma* 12(4):659–668
- [24] Nahum, A.M., and R.W. Smith (1976) An Experimental Model for Closed Head Impact Injury. *20th Stapp Car Crash Conference Proceedings*, 1976, Dearborn, MI.
- [25] DeWit, J.A., and D.S. Cronin. (2012) Cervical spine segment finite element model for traumatic injury prediction. *Journal of the mechanical behavior of biomedical materials* 10:138–150
- [26] Cronin, D.S., J.B. Fice, J.A. DeWit, and J. Moulton (2012) Upper Cervical Spine Kinematic Response and Injury Prediction. *2012 IRCOBI Conference Proceedings*, 2012, Dublin, Ireland.

- [27] Nightingale, R.W., J.H. McElhaney, D.L. Camacho, M. Kleinberger, B.A. Winkelstein, and B.S. Myers (1997) The Dynamic Responses of the Cervical Spine: Buckling, End Conditions, and Tolerance in Compressive Impacts. *41st Stapp Car Crash Conference Proceedings*, 1997
- [28] Funk, J.R., J.R. Kerrigan, and J.R. Crandall. (2004) Dynamic Bending Tolerance and Elastic-Plastic Material Properties of the Human Femur. *Annu Proc Assoc Adv Automot Med* 48:215–233
- [29] Untaroiu, C.D., J.B. Putnam, J. Schap, M.L. Davis, and F.S. Gayzik (2015) Development and Preliminary Validation of a 50th Percentile Pedestrian Finite Element Model. *Proceedings of ASME 2015 International Design Engineering Technical Conferences & Computer and Information in Engineering Conference*, 2015, Boston, Massachusetts, USA.
- [30] Kleiven, S., and W.N. Hardy. (2002) Correlation of an FE Model of the Human Head with Local Brain Motion—Consequences for Injury Prediction. *Stapp car crash journal* 46:123–144
- [31] Bain, A.C., and D.F. Meaney (1999) Thresholds for Mechanical Injury to the in Vivo White Matter. *43rd Stapp Car Crash Conference Proceedings*, 1999
- [32] Shen, M., F. Zhu, B. Jiang, V. Sanghavi, H. Fan, Y. Cai, Z. Wang, A. Kalra, X. Jin, C.C. Chou, and K.H. Yang (2015) Development and a Limited Validation of a Whole-Body Finite Element Pedestrian and Occupant Models of a 10-Year-Old Child. *2015 IRCOBI Conference Proceedings*, 2015, Lyon, France.
- [33] Dong, L., G. Li, H. Mao, S. Marek, and K.H. Yang. (2013) Development and validation of a 10-year-old child ligamentous cervical spine finite element model. *Annals of biomedical engineering* 41(12):2538–2552

VIII. APPENDIX

**Validation of Human Body Models**

The head of the GHBMCM50-O v4.3 model was validated with 35 experimental cases [17] including validation of brain pressure [18],[19] brain motion [20],[21] and behaviour of the skull bone [22],[23],[23]. The tolerance for brain contusions [24] was investigated reconstructing one case with and five cases without contusion. The peak maximum Von-Mises stress was 0.15 for the experiments of Nahum et al. [19]. The authors concluded that “Despite the need for further material tests and injury case reconstructions, the FE head model provides a solid method to predict and evaluate multiple head injuries for enhanced head safety countermeasures.” [17]

The cervical spine of the model was extensively validated [25],[26] using several load cases. One of them was the experiment of Nightingale et al. [27] – see Fig. 17.

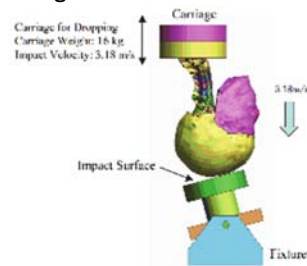


Fig. 17: Neck-Head Complex Validation [6]

In GHBMCM50-PS v1.3 head, upper extremities and the thorax were simplified to increase time efficiency and robustness. The model was validated with full scale impact tests of Kerrigan et al. against a mid-sized vehicle [28]. The lower extremities and the lumbar spine were also validated. No information on the validation of the cervical spine was available [29]. The head model of the THUMSAM50 v4.02 model was validated with most of the experiments GHBMCM50 was validated [19],[21],[23],[30], but no validations with the newer experiments of Hardy et al. [20] are published. The neck of the model was validated with experiments of Nightingale et al. [27] – see Fig. 17. The principal strain within the brain is proposed as a predictor for Diffuse Axonal Injury (DAI) with a reference value of 0.2 [9] based on [31]. The head-neck complex of CHARM-10 was validated against head-frontal impacts (with adult cadavers), head-drop and head-compression tests (pediatric cadavers). Neck flexion, tension and extension was validated at segment level (pediatric cadavers) and as a whole neck, using both pediatric and adult cadavers [32],[33].

**Validation of the Helmet Model**

The helmet model was validated against four experiments, two to the front and two to the side [1]. The helmet was fitted to a HIII 5<sup>th</sup> headform, which was dropped at 6.5 m/s against a flat anvil inclined by 30deg relative to the horizon – see Fig. 18. The anvil was covered with abrasive paper to increase tangential impact forces. Validation of the helmet was done with normal and misuse fit.

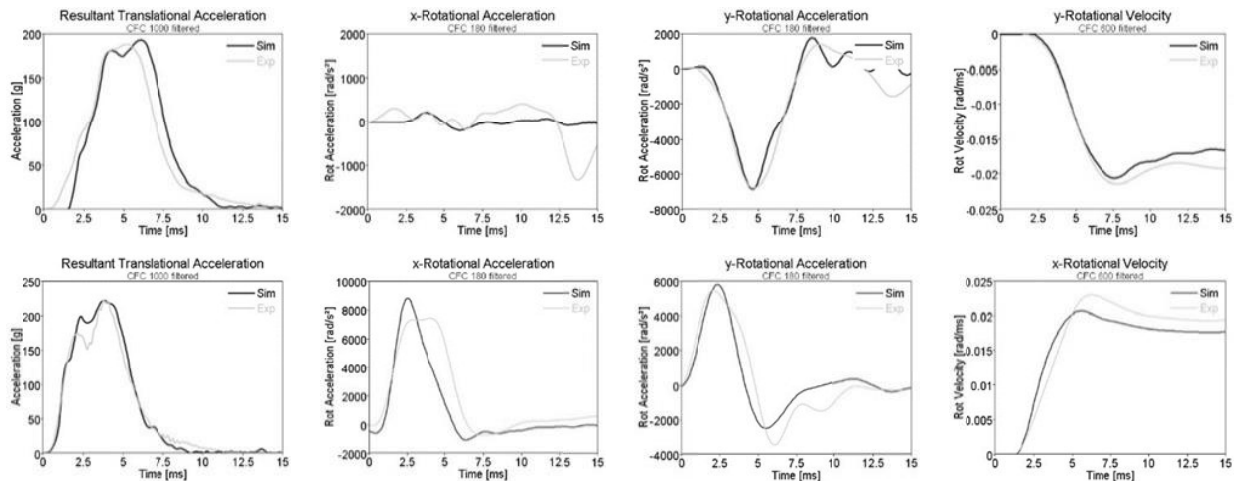


Fig. 18. : Validation of Helmet and Head combined. Frontal impact (upper row), lateral impact (lower row)

**Full Body Kinematics – Comparison of HBMs**

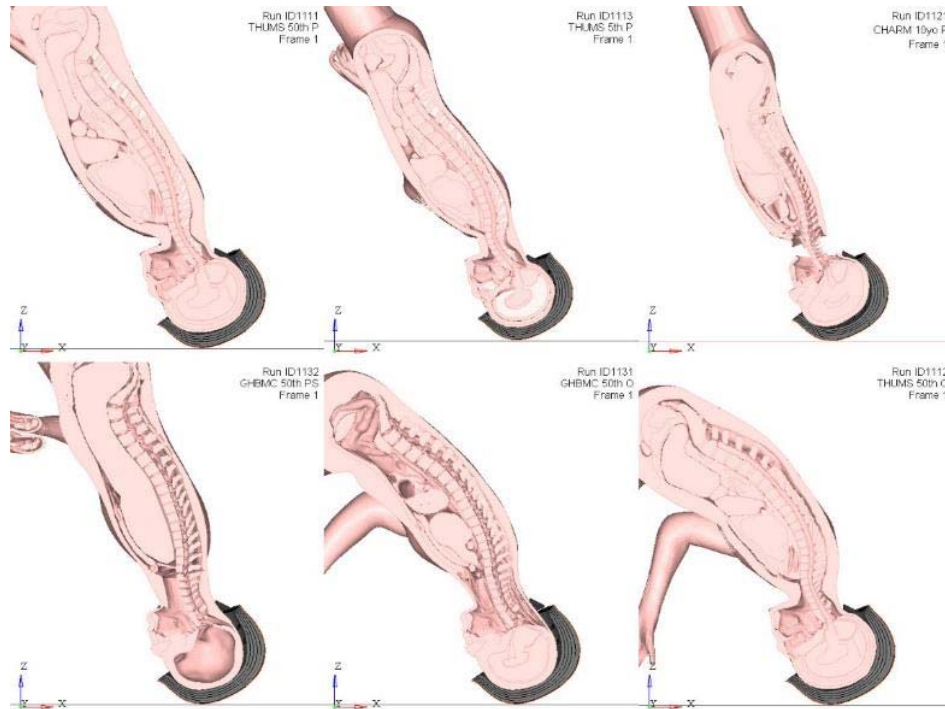


Fig. 19. Prior to impact – All models – impact configuration 11 (cross-section).

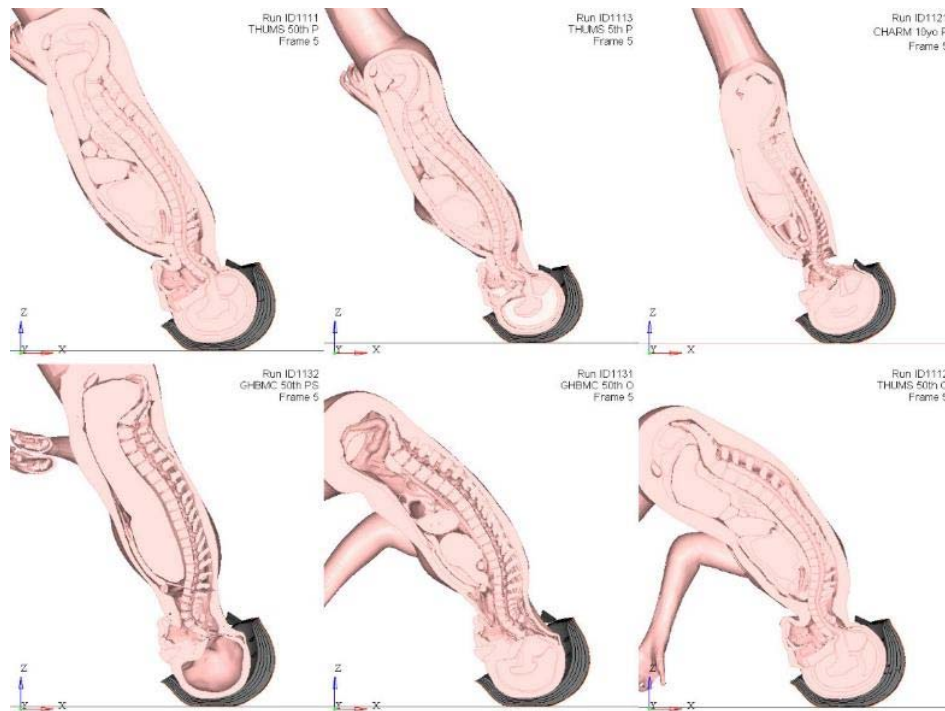


Fig. 20. Posture at 8 ms – All models – impact configuration 11 (cross-section).

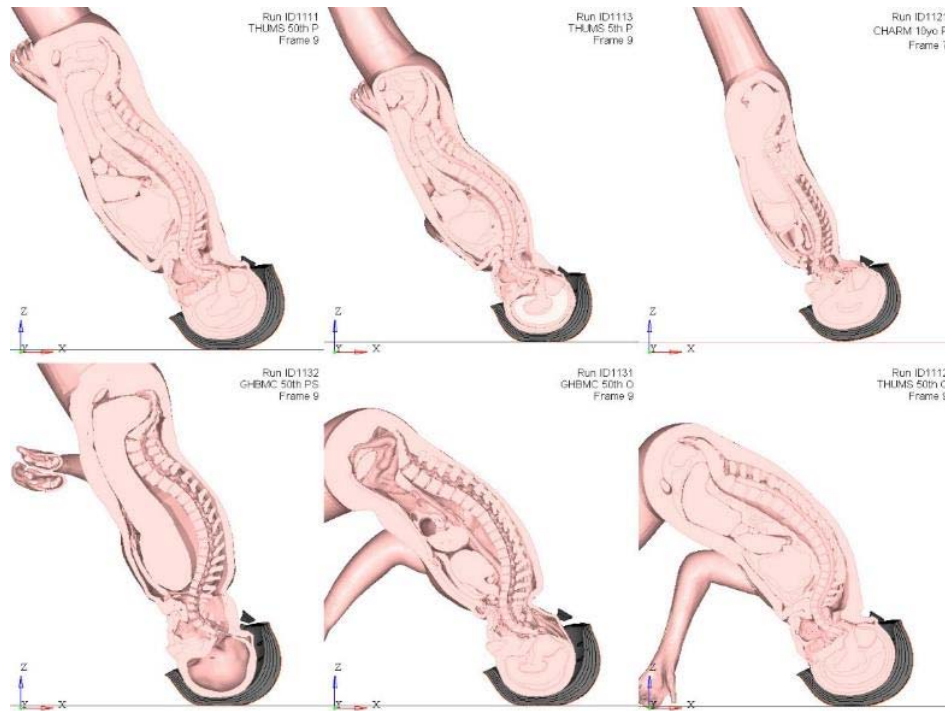


Fig. 21. Posture at 16 ms – All models – impact configuration 11 (cross-section).

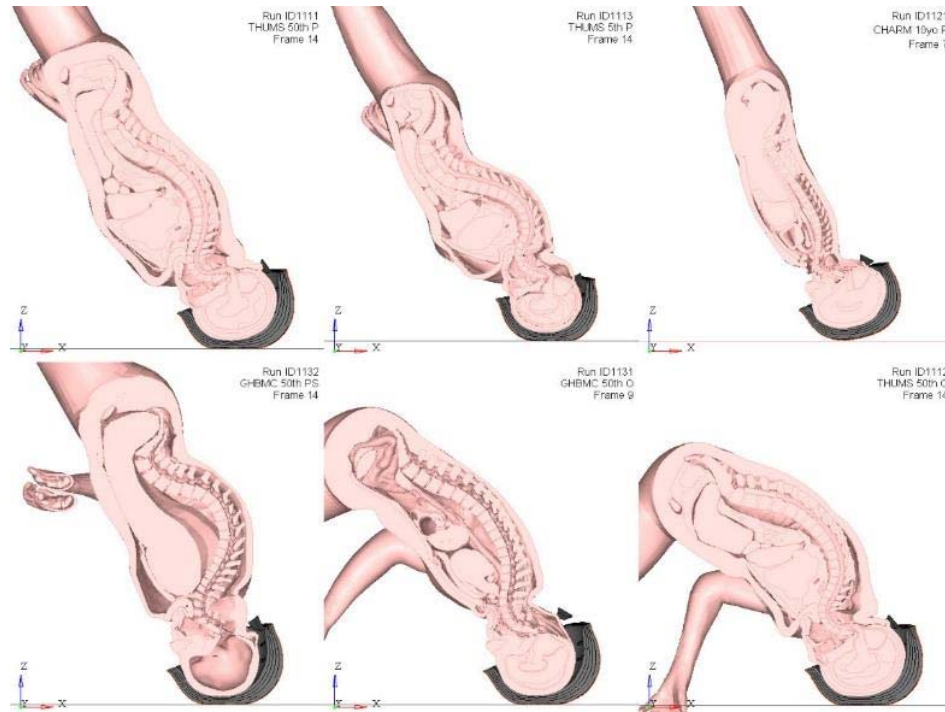


Fig. 22. Posture at 25 ms – All models – impact configuration 11 (cross-section).

**Full Body Kinematics – Comparison of Impact Scenarios**

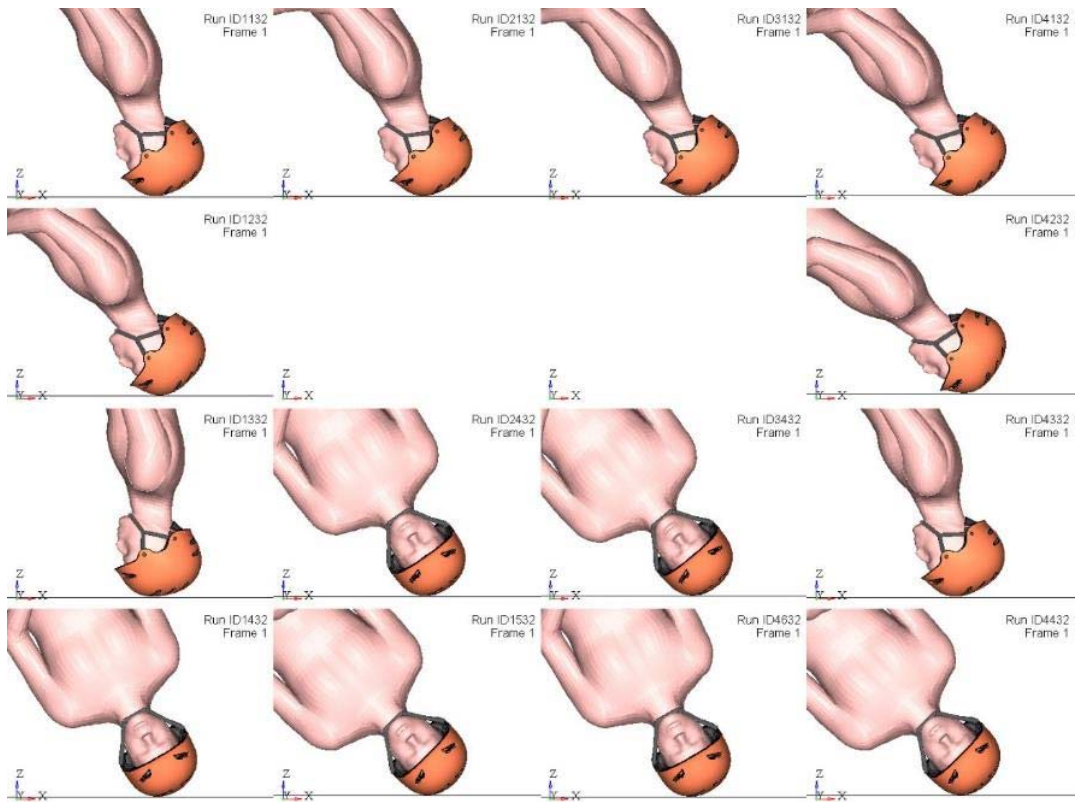


Fig. 23. Prior to impact – GHBM 50th PS – all impact configurations (Exterior).

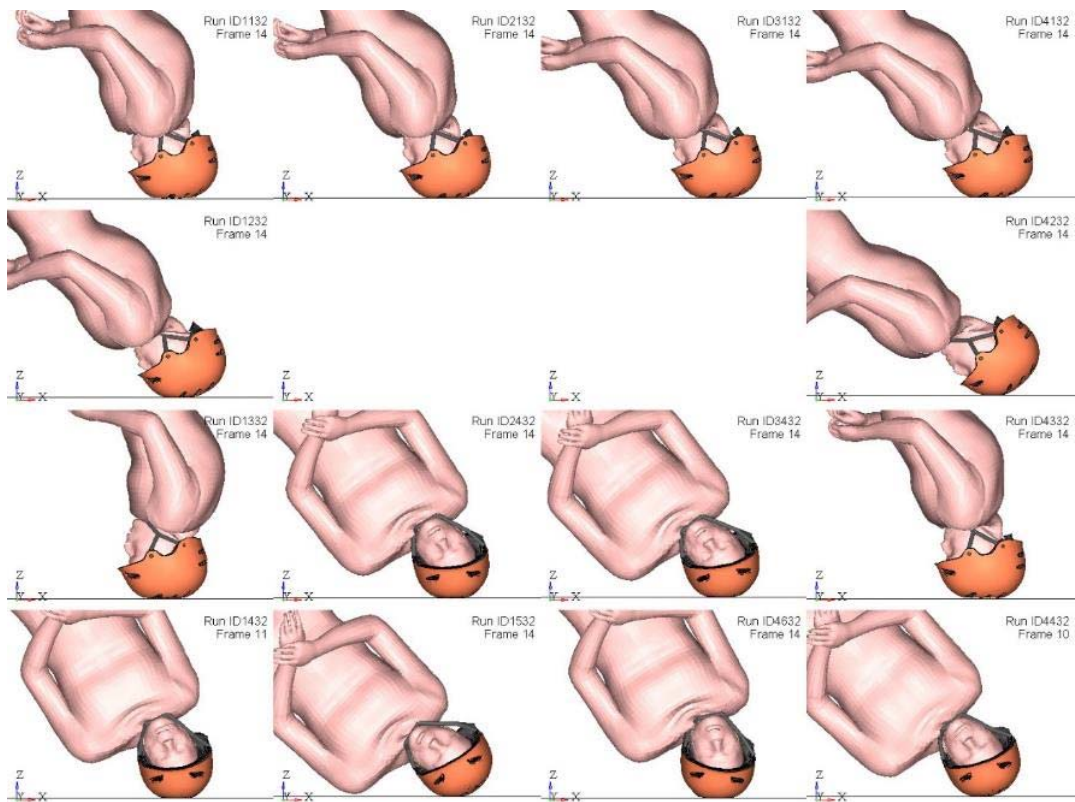


Fig. 24. Posture at 25 ms – GHBM 50th PS – all impact configurations (Exterior).

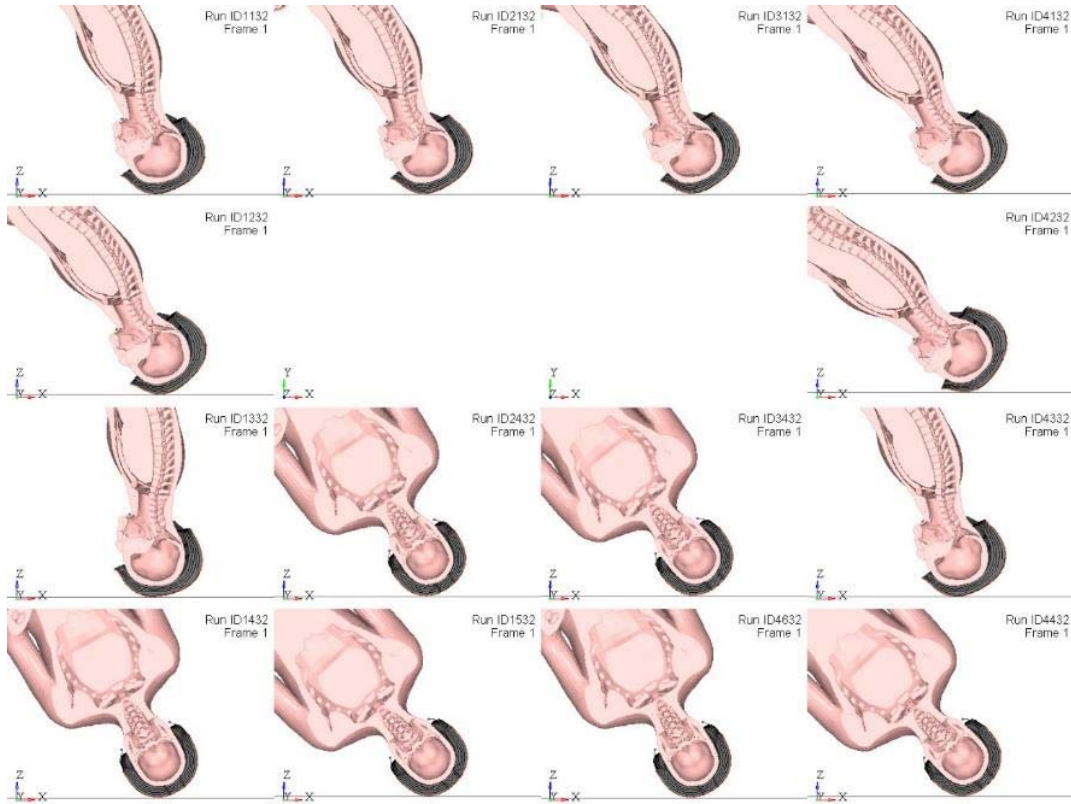


Fig. 25. Prior to impact – GHBM 50th PS – all impact configurations (cross-section).

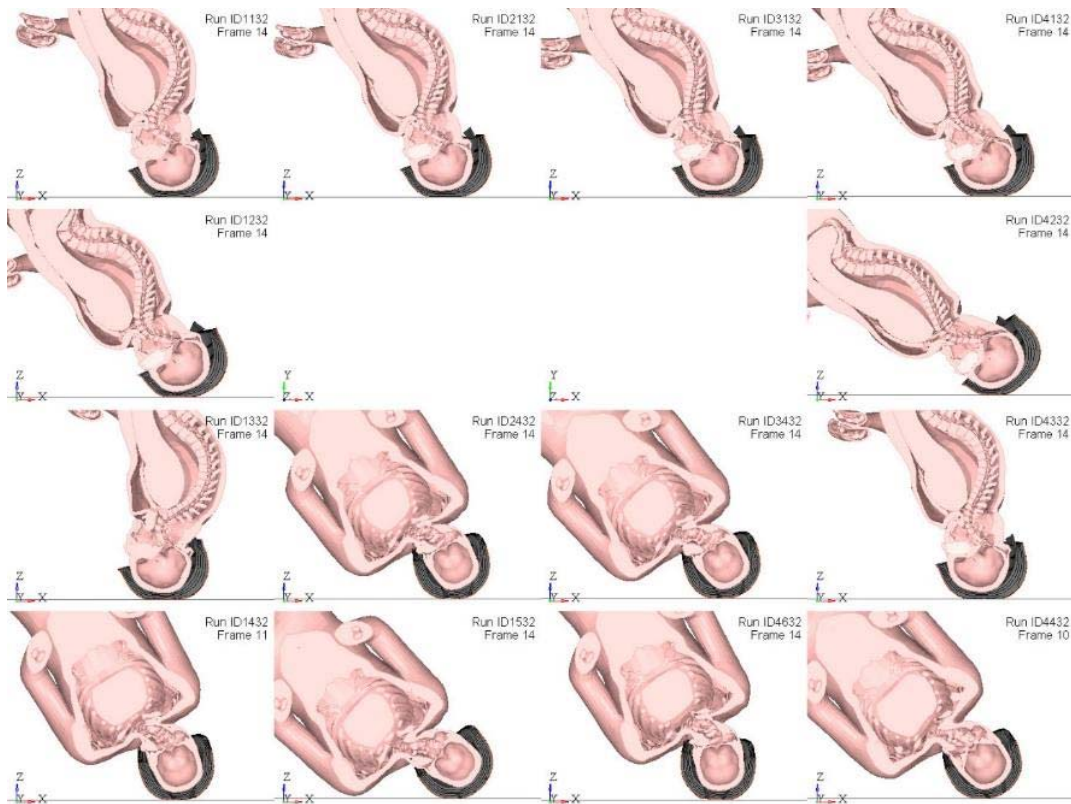


Fig. 26. Posture at 25 ms – GHBM 50th PS – all impact configurations (cross-view).

Maximum Principal Strains – Comparison of Models

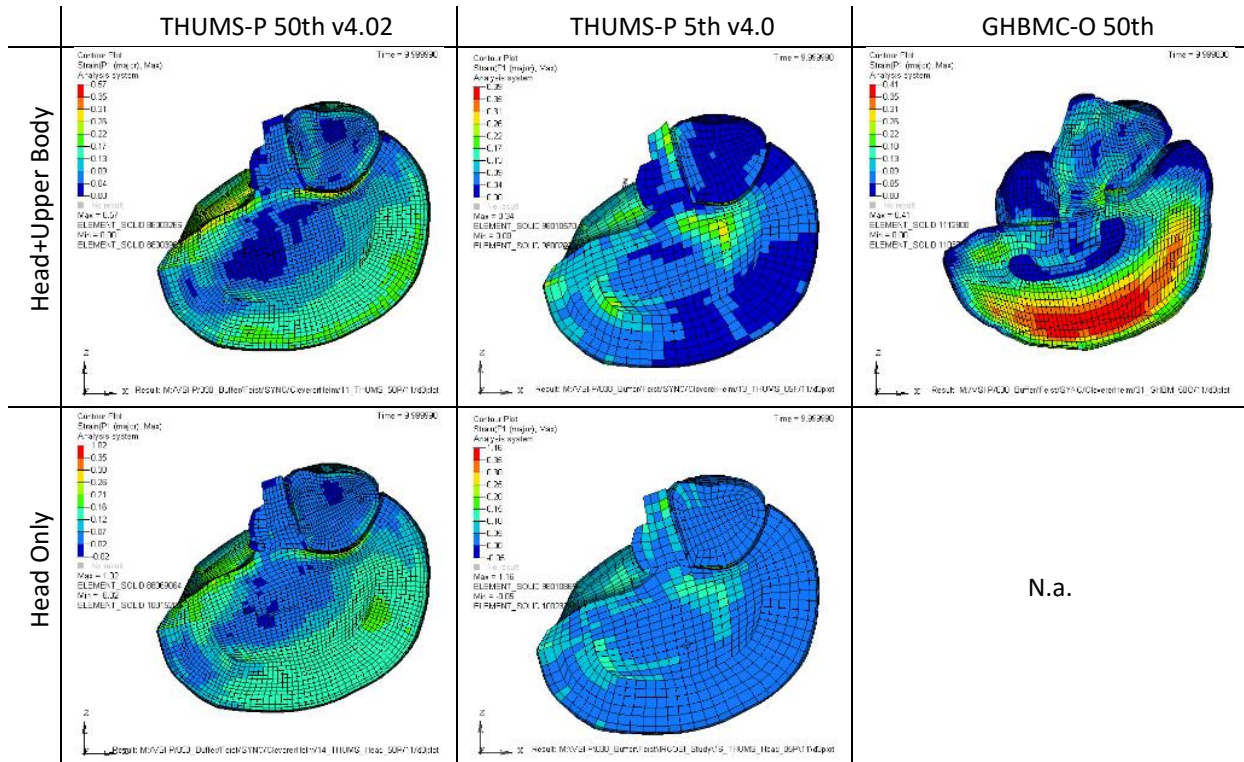


Fig. 27. Maximum Principal Strain in three different HBMs at 10 ms (Run 11), frontal impact

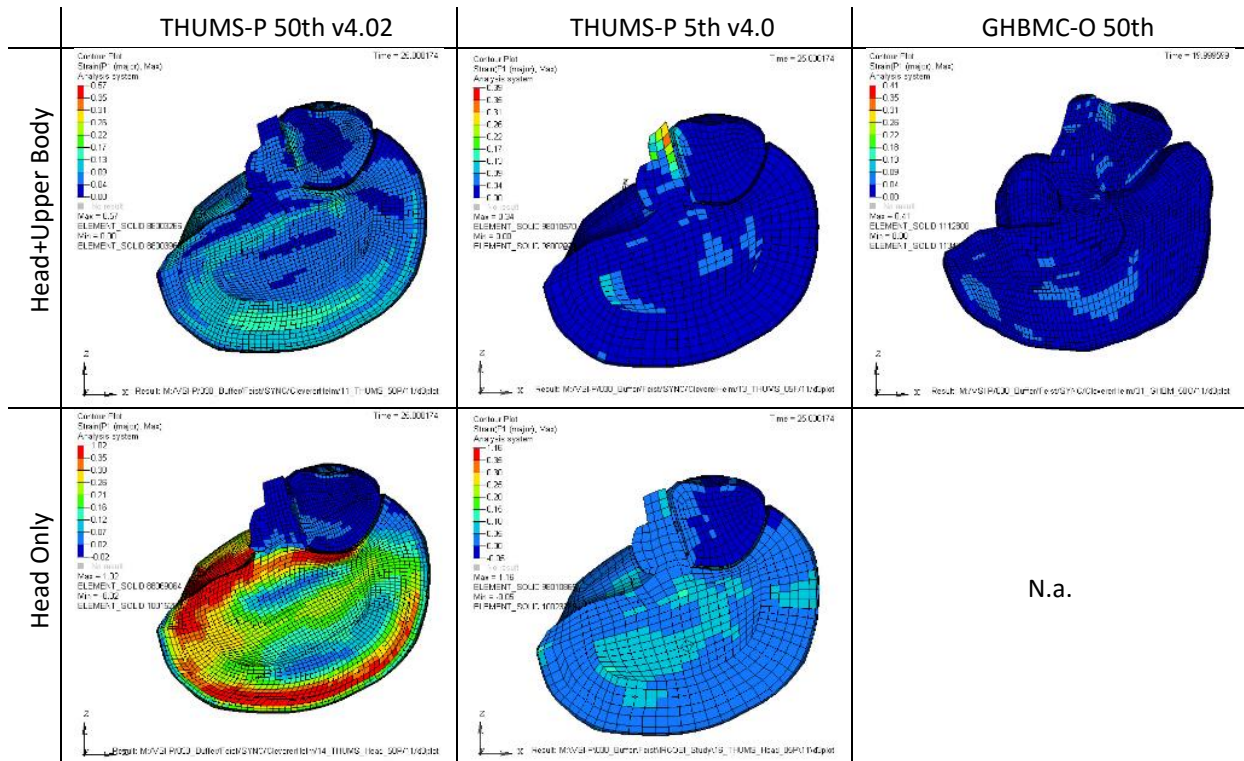


Fig. 28. Maximum Principal Strain in three different HBMs at 25 ms (Run 11), frontal impact

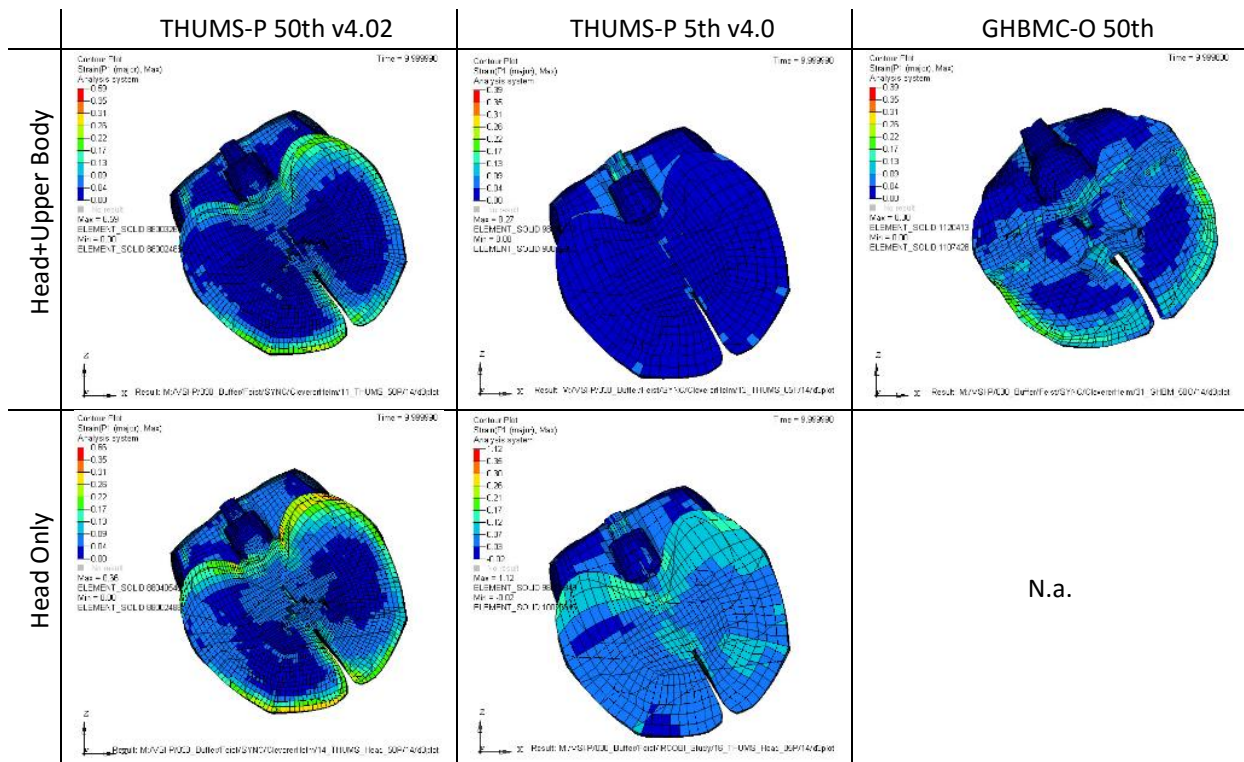


Fig. 29. Maximum Principal Strain in three different HBMs at 10 ms (Run 14), lateral impact

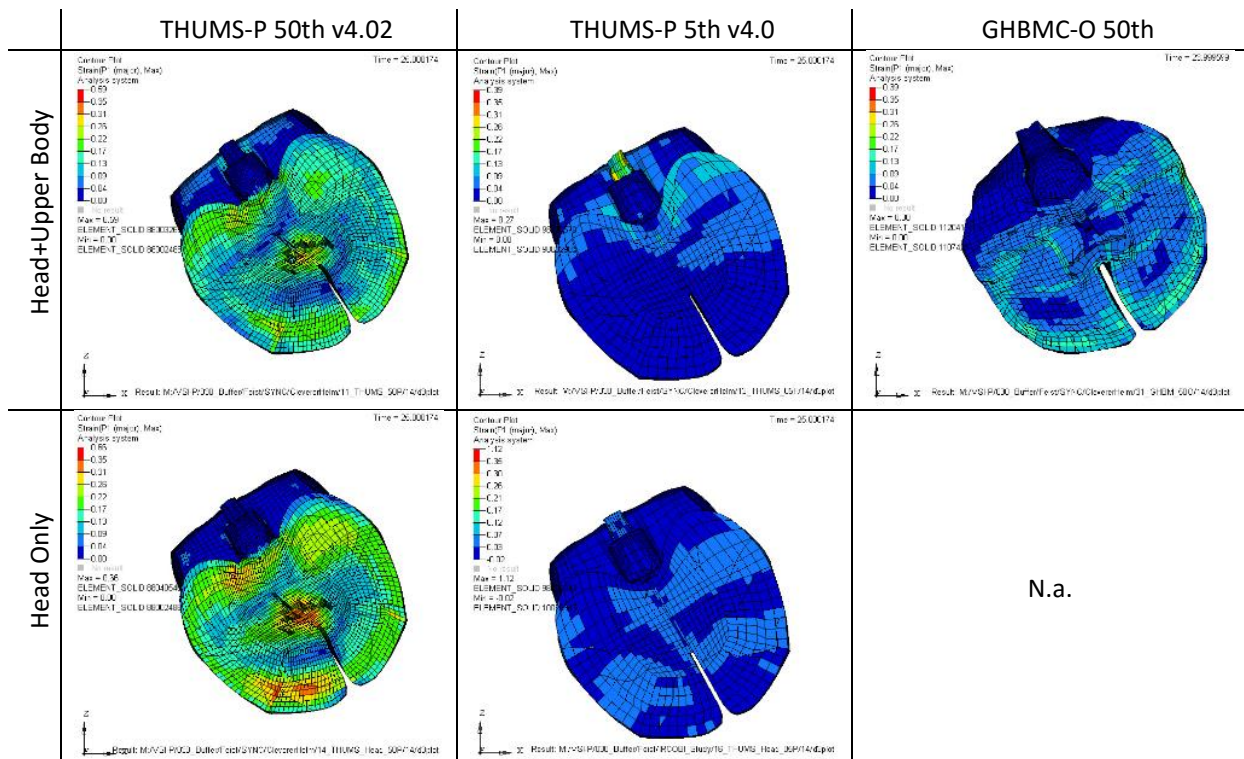


Fig. 30. Maximum Principal Strain in three different HBMs at 24 ms (Run 14), lateral impact

**Fitting of Helmets and Location of COG Sensors**

TABLE II  
 MASS, INERTIA AND HELMET-FITTING PARAMETERS

	THUMS 50th	THUMS 5th	GHBM 50th	CHARM	Remarks
Mass	5.4	3.37	4.4	2.91	
Ixx	23920	10867	18832	8055	
Iyy	29745	13267	22326	10465	
Izz	23083	10243	17383	9153	
COGx	-32	-14	-169	178.5	Coordinates in non-transformed HBM
COGy	0	0	0	204.6	CHARM supplied in non-standardised coordinate system (COGy≠0)
COGz	637	573	-692.3	56.8	
Measured in	Pedestrian	Pedestrian	Occupant	Pedestrian	
Frankfort Plane ry	7.3°	7.3°	0°	-10°	Pitch of Plane as provided by supplier — but transformed in a standardised coordinate system (consistent with THUMS v4.02 coordinate system)
Helmet-Head COG	29	29	29	17	Measured in helmet coordinate system
Helmet-Head COG	14	17	21.3	17.7	
Helmet Size	L	S	L	S	
Helmet-Head angle γ	7.3°	7.3°	7.3°	0.0°	